7-12-2016

Anomalous Fluctuations in the Orientation and Velocity of Swarming Bacteria

Shawn D. Ryan
Cleveland State University, s.d.ryan@csuohio.edu

Gil Ariel
Bar-Ilan University

Avraham Be'er
Ben-Gurion University of the Negev, beerav@gmail.com

Anomalous Fluctuations in the Orientation and Velocity of Swarming Bacteria

Shawn D. Ryan,[1] Gil Ariel,[2] and Avraham Be'er[3,*]

[1]Department of Mathematical Sciences, Kent State University, Kent, Ohio; [2]Department of Mathematics, Bar-Ilan University, Ramat Gan, Israel; and [3]Zuckerberg Institute for Water Research, The Jacob Blaustein Institutes for Desert Research, Ben-Gurion University of the Negev, Sede Boqer Campus, Midreshet Ben-Gurion, Israel

INTRODUCTION

Bacterial swarming is a collective mode of cell motion in which rod-shaped, flagellated bacteria rapidly migrate over surfaces (1–6). Swarming is associated with several biological manifestations such as cell elongation, increased flagellar density, secretion of wetting agents, and increased antibiotic resistance (7–13). During swarming, densely packed groups of bacteria move in coherent swirling patterns of whirls and jets that can persist for several seconds (14–21). Different experiments analyzing the dynamical swirling patterns of this group-phenomenon have mostly used video analysis methods (particle image velocimetry or optical flow) (14,15) to obtain a locally averaged velocity field describing the collective dynamical properties of the cells. These analyses include, for instance, the distribution of group velocities, spatial and temporal correlations, and clustering (14–17,22–24). In those studies much of the focus has been given to the physical interactions between cells and the medium, namely steric and hydrodynamic interactions, and the reduction of viscosity in crowded suspensions (14–17,23,25–27). For example, it was shown that dense suspensions of self-propelled rod-shaped bacteria are subject to orientational order instabilities that may be driving the vortexlike and irregular dynamic patterns of swarming bacteria (23,28–34). In other words, the collective swirling dynamics is a physical consequence of the mechanical characteristics bacteria exhibit during swarming.

However, despite considerable progress, the understanding of how the dynamics of individual cells scales up to give rise to the observed intricate collective dynamics is still lacking. Recently, by tracking trajectories of fluorescently labeled individuals within dense swarms, it was shown that wild-type (WT), self-propelled bacteria are performing superdiffusion, consistent with a realization of a Lévy walk. Lévy walks are characterized by trajectories that have straight stretches for extended lengths whose variance is infinite (35). This type of individual dynamics is fundamentally different from the one observed in the collective statistical properties of the same swarm (23,28,31,34,36–38).

Inside the active dense swarm, each cell contributes to its own, and to the collective's, motion by rotating its flagella to generate thrust. Several studies have shown that sparse WT swimming bacteria can migrate toward a nutrient source using a biased random walk controlled by a chemosensory signal transduction (39), following a regulated process called run-and-tumble. In contrast, the continuously circling motion of individual WT bacteria within an expanding swarm is not directly controlled by the chemotactic signaling system (2). The fact that swarming bacteria do not follow simple run-and-tumble dynamics is also manifested in their

superdiffusive behavior (35). Nonetheless, the ability to exhibit various maneuvers during flagellar rotation, either through interactions between adjacent cells, or because of other yet-undiscovered reasons, turns out to play a major role during swarming; as a result, the contribution of self-propulsion of an individual cell to its final trajectory in a crowded colony was unclear.

Here, by simultaneously tracking the flow of the entire swarm and the motion of individuals within it, the patterns of the two motions can be compared and analyzed. We show that WT motile cells do not strictly follow the collective flow and may swim perpendicular or even against it. Moreover, the angle between the elongated cell axis (cell-orientation) and the flow, measured precisely at high magnification, shows large deviations. This is in contrast to immotile cells embedded within an active swarm, which typically follow the collective stream lines and are orientated parallel to the flow. A small correlation between the orientation of the WT cell and the local velocity field of the flow has been previously observed in bacteria swimming in a free-standing soap-film set (25). This effect has been attributed to the interplay between the bacteria pushing in the direction of its axis while simultaneously being advected by the flow generated by the entire swarm.

One of the main objectives of this article is to further study and quantify this effect and the mechanisms underlying it. The comparison between the single-cell and the collective dynamics allows a quantitative examination of the different forces that underlie bacterial swarming—what are the key physical interactions, what is the role of spatial and rotational diffusion, and more. In particular, we show that the difference between WT and immotile cells is also observed in a qualitatively different distribution of fluctuations—while the deviation of the cell orientation and velocity direction compared to the collective flow is Gaussian-like for immotile cells, WT bacteria show anomalous fluctuations. Therefore, the contribution of individual self-propulsion of a cell, within the active swarm, is more than simply generating movement forward and may be related to the ability of cells to maneuver between streams. As we demonstrate below, these differences are particularly important in the design of theoretical models of swarming bacteria and their simulation. For example, simplified models of swarming bacteria as elongated pushers/pullers can be compared to our experimental observations and analyzed accordingly. In the following, we reexamine the model of Ryan et al. (40–42) in which the effect of a cell on the surrounding liquid is represented as a hydrodynamic force dipole. We find that to explain the dynamics as observed in our experiments, the model needs to be adjusted. In particular, a minimal model has to take into account steric repulsion, alignment, and hydrodynamic interactions. On the other hand, several other suggested mechanisms do not generate dynamics, which is consistent with our experiments. In this sense, our results expose the relevant mechanisms underlying bacterial collective dynamics.

From the biological point of view, our results demonstrate that the dynamically swirling swarm serves as a complex background flow to cells. In particular, it does not fully describe the dynamics of individuals, which can actively push and hop between jets. The nature of the fluctuations (von Mises, or non-Gaussian) is a precursor of the fact that the observed deviations among the collective flow, cell orientation, and cell velocity are not due to random fluctuations or noise, but are an essential aspect of bacterial dynamics.

MATERIALS AND METHODS

Bacterial strains and growth protocol

Experiments were performed using two bacterial species. The first was *Bacillus subtilis* strain 3610 (WT), which is a Gram-positive rod-shaped (0.8×5 μm) species, used as a model system in many previous quantitative swarming experiments (1–4,7,11,14–17). The cells were grown on agar plates (1 g/L peptone and 0.5% agar at 30°C); cells formed dense colonies (thickness of 3–4 μm) and began expanding outwards at ~4 h after inoculation. Note that these conditions are different from published protocols that use LB and where cells swarm in a monolayer and expand out earlier (1). A derivative strain of 3610 was labeled with a red fluorescent protein (RFP), where the protein was expressed from a chromosomal location (*ppsB*::P*trpE*-mCherry). The WT were mixed with the RFP variant (at a ratio of 100:1) in a small tube before inoculation, then coinoculated on swarm agar plates. Labeling does not affect swarming behavior (35). Under fluorescent microscopy only RFP cells are seen, which enables a precise detection of single-cell trajectories even within a highly dense population.

The second bacterial system used was *Serratia marcescens* strain 274 (WT), which is a Gram-negative rod-shaped (0.8×4 μm) species, used as a model system in previous swarming experiments (1,7,11,24). The cells were grown on agar plates (LB and 0.5% agar at 30°C); cells formed dense colonies (vertical thickness of 3–4 μm) and began expanding outwards at ~5 h after inoculation, and swarmed rapidly (~20 μm/s). To track individuals, *S. marcescens* were labeled with a green fluorescent protein (GFP) expressed from a plasmid (pTRC99a::GFP; strain JP1020). Similar to experiments with *B. subtilis*, WT and GFP-labeled strains were mixed at a ratio of 100:1 before inoculation on agar plates. GFP-labeled immotile bacteria (strain RH1037 that lacks the flagellar filament gene *hag*) were mixed with the population of unlabeled WT at ratio of 100:1.

Fluorescently labeled immotile cells were added to the swarm using several different protocols that all yielded essentially the same results; however, some were simply more convenient to use than others were. Note that joint inoculation of motile and immotile cells was not successful because immotile cells did not migrate to the colony's edge where WT swarming is most pronounced.

The first protocol, which was found to be the most reliable and easy and upon which our results are based, was by growing small immotile colonies next to a larger swarming colony of WT cells; these were inoculated at the plate-center earlier. The two colonies merge spontaneously.

In the second protocol, small colonies (~20% of the WT volume, i.e., 1 μL) of immotile cells were inoculated near the envelope of an expanding WT colony. The drop inoculation of the small colonies never touched the large colony. When the small colony was dry due to absorption to the agar, the distance between the interfaces of the colonies was <100 μm, and the plates were immediately taken for observation. Many small colonies were inoculated this way at random distances and few were successfully set to be at the right distance. For control, the same procedure was repeated by using fluorescently labeled WT cells for the small colonies instead of mixing them in a small tube before inoculation, yielding identical results.

In a third protocol, immotile cells were embedded in WT supernatant before inoculation. The immotile cells were washed by gentle centrifuging, removing their supernatant. Then, WT-filtered (0.2 μm) supernatant at the same volume was added to prevent sticking to the surface. The results of both methods, with or without changing the supernatant, were the same.

All bacteria were stored at −80°C in 50% glycerol stocks (antibiotics were added to frozen stocks of the RFP and GFP mutants; phleomycin for *B. subtilis* (7 μg/mL) and ampicillin (100 μg/mL) for *S. marcescens*), selected on an LB plate (with the appropriate antibiotic) and grown overnight in LB broth at 30°C and shaking (200 RPM) before plate inoculation (5 μL at the center of each plate).

Observations

Optical microscopy (Axio Imager Z2; 63× lens; Carl Zeiss, Jena, Germany), equipped with a sensitive high-resolution video camera (NEO; Andor Technology, Belfast, UK), was used to capture the motion of the labeled cells under fluorescence microscopy (50 frames/s and 1024 × 1024 pixels). Trajectories were obtained and analyzed using MATLAB (The MathWorks, Natick, MA). For both bacterial species, no photobleaching was observed during acquisition times (2 min for each experiment: 6000 frames). In each field of view, we typically had approximately 5 labeled cells at 63× and 50 labeled cells at 20×. The total data summarizes results from tens of experiments with hundreds of cells from each species. Because standard fluorescent light strongly affects cell motility (it usually completely stops their motion in <1 s), we used a slightly modified version for the filters and dichroic mirror. The GFP-labeled cells were observed by a standard yellow fluorescent protein (YFP) Carl Zeiss illumination setup instead of the standard GFP one (Filter set 46 YFP shift-free: Excitation 500/25; Beam Splitter 515; Emission 535/30). The cell intensity was slightly weaker compared to GFP. The RFP-labeled cells, designed initially for mCherry illumination setup, were observed by standard Rhodamin (RFP) (Filter set 20 Rhodamin shift free: Excitation 546/12: Beam Splitter 560; Emission 607/80; Carl Zeiss).

A second camera (GX 1050: Allied Vision Technologies, Newburyport, MA) detecting simultaneously the exact field of view by phase contrast illumination, was operated at 100 frames/s and same spatial resolution. The series of images capturing the motion of all bacteria in the field of view (not only fluorescently labeled ones) were analyzed by standard optical flow measurements (kindly see more details below, and those of Benisty et al. (14) and Rabani et al. (24)).

Smoothing of trajectories

Trajectories were smoothed using MATLAB's "malowess" function, which locally fits a polynomial (second order) to a moving window (11 frames).

Optical flow

Our flow analysis methods have been previously applied and described in Benisty et al. (14) and Sokolov and Aranson (22). Following standard preprocessing for noise reduction. the optical flow between each of two consecutive frames was obtained using the Horn-Schunck method (43). Vector fields were smoothed using an exponential kernel in time (exponent 0.8) and a diffusive kernel in space (the central weight is 0.6). Reducing to a 64 × 64 grid generated an approximated velocity field. Different smoothing, coarsening, or restriction to smaller regions yielded similar results.

RESULTS

Fluorescently labeled *Bacillus subtilis* cells expressing RFP were mixed with their WT-unlabeled parent strain at a ratio of ~1:100 and coinoculated on swarm agar plates. The bacteria grow into a dense, motile colony, which begins expanding outward after 4 h and covers the agar plate after a further 3 h. We focused on the outer regions of the expanding swarm where the colony has multiple layers (~3 μm thick), and the cells are more active (Fig. 1 *A*; Movie S1 in the Supporting Material). For each of the species, data was collected from 20 different experiments, yielding trajectories of nearly 500 cells that altogether have generated >10,000 instantaneous data points. All the experiments described below were repeated with a different swarming species, *Serratia marcescens*, which yielded essentially the same results. See Fig. S1 for examples of reproducibility and differences between the two species.

Under phase contrast illumination, the velocity and vorticity fields of all swirling bacteria in the swarm were obtained by optical flow analyses (14). A typical dynamical pattern of the collective vortices and jets is seen in Fig. 1 *B*. Simultaneously and at the exact same field of view, single labeled cells migrating within the swarm were detected by fluorescence microscopy (Fig. 1 *C*; Movie S2). Example trajectories are depicted in Fig. 1 *D*. At this magnification (63×), a single bacterium covers ~1000 pixels, which ensures a precise detection of cell location and trajectory, as well the cell's shape, size, and orientation. Fig. 1 *D* depicts an example of the superposition of the collective velocity field of the swarm (*parallel black arrows*), the orientation of the rod-shaped cell (*pink solid line*) and the instantaneous cell velocity marked by a red arrow (tangent to the trajectory). See also Movie S3.

As a control experiment, RFP-labeled immotile cells were mixed with swarming WT bacteria. Immotile cells are similar to the WT and differ only in the absence of flagella. Thus, any motion of an immotile cell embedded in a WT active swarm is necessarily due to the flow around it, possibly thermal fluctuations and measurement errors. Therefore, the motion of immotile RFP-labeled cells takes into account only the effect of the swarm and the fluid on an individual of a similar shape and size. Fig. 2 *A* shows the angular difference between the direction of motion of immotile cells embedded in a WT swarming colony and the local flow around it. Typically (in >90% of the cases), the difference between the direction of the flow and the direction in which an immotile cell is actually moving is <22°. Angles larger than 40° were never observed. Similarly, Fig. 2, *B* and *C*, shows that cell orientation is almost always parallel (up to ~20°) both to the direction of motion and to the flow. Moreover, the distribution fits well a von Mises distribution (the circular analog of the Gaussian distribution), indicating that the orientation of cells is governed by the flow, up to random fluctuations. These results provide an estimate of the errors in our directional measurements. These include errors due to spatial and temporal smoothing that are an unavoidable stage of the optical flow algorithm and measurement errors.

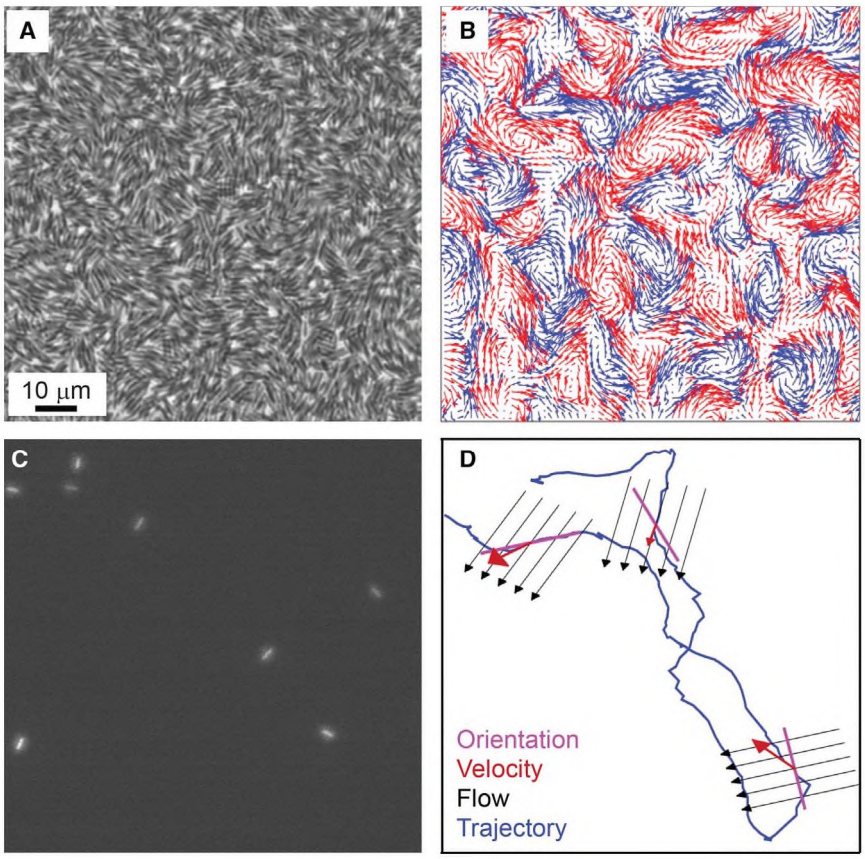

FIGURE 1 Observations of collective and individual dynamics of swarming bacteria. (*A*) Phase-contrast imaging of a WT *B. subtilis* swarming colony at high magnification, taken close to the colony edge. (*B*) The instantaneous velocity field at the same time. Colors indicate clockwise (*red*) or counterclockwise (*blue*) motion. (*C*) Fluorescent microscopy shows only the fluorescently labeled bacteria, at the same field and time. (*D*) An example trajectory of an individual bacteria (*blue line*), superimposed with the collective flow (*black arrows*), cell orientation (*pink bar*), and instantaneous cell velocity (*red arrow*). To see this figure in color, go online.

In contrast to the immotile bacteria, individual WT cells moving within the swarm exhibited a different distribution of angular difference among their movement direction, the collective flow, and cell orientation. For example, as seen in Fig. 2 *A*, the median angle between the local flow and the actual cell velocity was 40°. Similarly, in Fig. 2 *B*, showing the angle between the cell orientation and the actual cell velocity, the large majority of measurements show an angle larger than 22°. Fig. 2 *C* shows the angle between the local flow and the cell orientation. The distribution is fairly uniform, indicating that the direction of the flow and the cell orientation are close to independent. Moreover, the von Mises distribution fits the results poorly. This clearly demonstrates the significant differences between immotile and WT cells while moving inside the active swarm, and exposes the complex importance of self-propulsion of the cells.

To further characterize the dynamics of WT cells within a swarm, we study the correlations between different measured

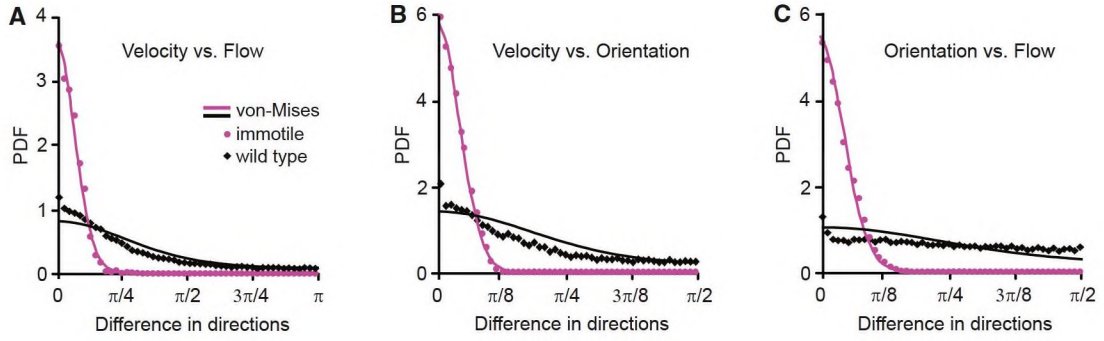

FIGURE 2 Differences in directions: experimental results. (*A*) Distribution of angles between the cell velocity and the flow vector field at the same position and time. Immotile cells (*pink circles*) move with the flow while WT cells (*black diamonds*) exhibit much larger deviations. (*B*) Distribution of angles between the cell velocity and its orientation. Immotile cells tend to be aligned with the actual direction of motion while WT bacteria exhibit significantly larger deviations. (*C*) Distribution of angles between cell orientation and the flow vector field at the same position and time. Immotile cells tend to be aligned with the flow while WT exhibit large deviations. (*Solid lines*) Maximal-likelihood fit to a centered von Mises distribution. To see this figure in color, go online.

quantities. For each of the cells analyzed, we calculate pair correlations among three quantities: 1) the angle between the velocity direction and the flow (i.e., the cell direction compared to the flow); 2) the angle between the cell orientation and the flow (i.e., the positioning of the cell body compared to the flow); and 3) the local vorticity, defined as the absolute value of the curl of the flow vector field. Fig. 3 shows the distribution of correlations between velocity-orientation, velocity-vorticity, and vorticity-orientation among cells. In other words, the figure shows how correlations vary among different cells. On average, the vorticity is independent of the relative velocity and orientation of cells, indicating that cells are equally likely to move with the flow or move against it, regardless of whether it is in a vortex (high vorticity) or in a jet (low vorticity). However, the correlation between the velocity direction and the orientation (compared to the flow) is high, indicating that typically, either all directions (flow, velocity, and orientation) are aligned, i.e., the cell is oriented in the direction of the flow and is moving along it, or the three directions are independent.

Modeling

The experimental results have clearly shown a major difference between the motion of WT and immotile cells embedded in active swarms. To identify the principle interaction underlying our experimental results, we introduce a simplified model that approximates the translational and rotational degrees of freedom for each cell by determining the balance of forces and torques on it. Various approaches have been proposed to study swimming bacteria by modeling each as a slender body (44), a dumbbell (45), or a hydrodynamic point dipole (40–42); we adapt the latter approach.

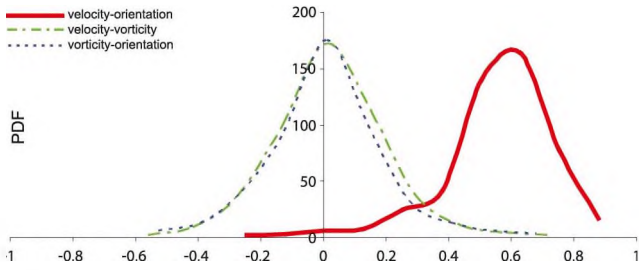

FIGURE 3 Distribution of correlations. For each cell analyzed, three data sequences were analyzed: 1) the angle between the velocity direction and the flow, 2) the angle between the cell orientation and the flow, and 3) the vorticity at the cell location. The (Pearson) correlation coefficient for each pair was calculated (individually for every cell). The figure shows the distribution of correlations among cells. On average, the vorticity is independent of the relative velocity and orientation of cells, indicating that cells are equally likely to move with the flow or move against it regardless of whether it is in a vortex (high vorticity) or in a jet (low vorticity). The high correlation between the velocity direction and the orientation (compared to the flow) indicates that typically, either all directions (flow, velocity, and orientation) are simultaneously aligned, or they are random. To see this figure in color, go online.

From an individual cell perspective, we expect slender bodies or dumbbells to produce a similar result, but the point dipole model offers several advantages. Namely, there is an analytical solution for the flow generated by a single dipole. While this is not the exact flow generated by a real cell, it is qualitatively close (e.g., compare the experimental measurement of the flow of a single cell (46) to point dipolar flow in Ryan et al. (42)). The point dipole model was also chosen for its simple nature while still accounting for long-range hydrodynamic interactions and near-field collisions. Because the motion and orientation of the cells crucially depend on the flow generated from others, it is important to have a large number of cells resembling the bulk in the experiments. Thus, an analytical expression for the flow greatly reduces the computational time needed for evolving each cell in contrast to solving the fluid equations numerically, and allows for the simulation of a large number of cells in a shorter period of time.

In this two-dimensional model, N bacteria are represented by the location of its center of mass, x_i, and its orientation vector d_i, $|d_i| = 1$, $i = 1, \ldots, N$. The vector field describing the instantaneous flow of the liquid surrounding the cells at position x and time t is denoted $u(x,t)$. Assuming overdamped dynamics, the center of mass is given by

$$\dot{x}_i = v_i d_i + u(x_i,t) + \beta \sum_{j \neq i} F(x_i - x_j). \tag{1}$$

The first term on the right-hand side describes the forward thrust, pushing the cell with force v_i, which, in general, may be different for different cells. The second term describes advection by the flow. The third term describes short-range steric interaction between cells. For simplicity, we assume a truncated repulsive potential of Lennard-Jones type that repels particles within one particle length $l = 5\ \mu$m (the width of a cell is taken to be 1 μm). Other choices of purely repulsive potentials, for example, an exponential Yukawa potential, could be used as well.

The cell orientation, d_i, is given by instantaneous alignment to a vector field $G(x_i, d_i)$ that also depends on the fluid flow u, with noise. More precisely, advancing the system with step size Δt, d_i is given by

$$d_i(t + \Delta t) = \begin{pmatrix} \cos \xi_{i,n} & \sin \xi_{i,n} \\ -\sin \xi_{i,n} & \cos \xi_{i,n} \end{pmatrix} \widehat{G}(x_i,t). \tag{2}$$

The matrix in Eq. 2 is a rotation matrix with independent random angles $\xi_{i,n}$ drawn from the von Mises distribution with zero mean and width parameter $\kappa/\Delta t$. The normalized vector field $\widehat{G}(x,t)$ is a sum of two contributions:

$$\begin{aligned} G(x,t) &= u(x,t) + \Delta t J(x,t) \\ \widehat{G} &= G/|G|, \end{aligned} \tag{3}$$

where $|G|$ denotes the Euclidean norm of a vector G. The first term in Eq. 3, $u(x,t)$, implies that cells align with the

flow direction. The second term describes rotation due to the shear flow created by the propulsion of the other cells. This shear can rotate the elongated cells. Using Jeffery's equation (47), the rotation of an ellipsoid with direction d_i (in three dimensions) is given by

$$\dot{d}_i = -d_i \times \left[w\nabla \times u + \frac{B}{2} d_i \times (\nabla u + \nabla u^T) d_i\right], \quad (4)$$

where B is the Bretherton constant for an ellipsoid with principle radii a and b, $B = (b^2 - a^2)/(b^2 + a^2)$. For example, $B = 1$ for needles and $B = 0$ for spheres. In two dimensions, the first term, describing the local vorticity, does not create rotation in the x-y plane and can therefore be removed. As a result, the force exerted by the shear is

$$\Delta t J(x,t) = -\frac{B}{2}(\nabla u + \nabla u^T) d_i. \quad (5)$$

Note that a constant flow does not rotate the particle. Lastly, we assume that each cell is effectively a hydrodynamics dipole. Assuming that the suspension is in a so-called semi-dilute regime, the total flow is a sum of the individual flows created by all the other motile cells. Given the swimming speed, characteristic length, and ambient fluid viscosity, the suspension is in the low Reynold's number regime, $Re << 1$. As a result, fluid in the suspension can be modeled via an incompressible Stokes equation with contributions from each of the active swimming cells. Then, it can be shown (42) that $u(x,t)$ is given by

$$u(x,t) = -\frac{l_1}{3\pi} \sum_{j=1}^{N} \left(\nabla^3 \left[log\left(|x - x_i|\right)\right] \cdot d_j(t)\right) p_j d_j(t), \quad (6)$$

where p_j is the dipole moment of cell j ($p_j > 0$ for pushers, $p_j < 0$ for pullers, and $p_j = 0$ for immotile cells) and l_1 is the film thickness. Note that in quasi-two dimensions, the fluid flow created by a single dipole decays as the cube of the distance, rather than the quadratic decay in three dimensions. This enhanced decay of the fluid velocity is due to the effect of confinement.

The dipole solution Eq. 6 can be derived from the flow of a monopole in a confined thin film model (48) relying on the important feature that the thickness of the film is much smaller than the other two dimensions. Taking two oppositely oriented force monopole flows and keeping the leading-order term in the Taylor expansion in the limit of a zero separation, l, yields (42)

$$\mathbf{u}_{\text{dip}}(\mathbf{x}) = \lim_{l \to \infty} \left[\mathbf{u}_{\text{mono}}\left(\mathbf{x} + \frac{l}{2}\mathbf{d}\right) - \mathbf{u}_{\text{mono}}\left(\mathbf{x} - \frac{l}{2}\mathbf{d}\right)\right]. \quad (7)$$

While our experimental setup has a similar thin film between a bottom agar layer and the top is open air, the accumulation of bacteria metabolism products can result in a no-slip boundary condition on the top surface of the film. These metabolic products secreted by *B. subtilis* create an enhanced surface tension and elasticity on the film surface, resulting in a solid boundary (23).

In simulations, $N = 6400$ are used in a rectangular domain with periodic boundary conditions. With a system size $L = 100l$, the effective volume fraction is $N\pi l^2/4L^2 = 0.503$, which is comparable to the density in experiments. This regime captures the behavior of the suspension in the bulk far from the walls while greatly reducing any finite domain effects. Nondimensional parameters for particles representing WT cells are $v_j = v = 0.1$ and $p_j = F_p l = \zeta \eta l^2 v_j$ (the propulsion for F_p is proportional to the isolated swimming force v_j, and the ambient viscosity is η through an effective Stokes drag law with the coefficient ζ determined by the shape). In the simulations, $\zeta\eta = 1$. In simulations with immotile cells, all particles are WT except for 10 test particles for which $v_j = p_j = 0$. The random noise $\xi_{i,n}$ is assumed to have a von Mises distribution with density $e^{\kappa \cos\theta}/(2\pi I_0(\kappa))$, where $I_0(\cdot)$ is the zeroth Bessel function of the first kind. In the simulations we chose, $\kappa = (24/\pi)^2$ to fit the noise in the immotile case. See Table S1 for a list of all model parameters, the values used in simulations scaled to physical units, and a brief description of the reasoning for choosing them.

Fig. 4 depicts simulation results with parameters corresponding to experiments. Note the similarity to the experimental results in Fig. 2; in particular, the Gaussian (von Mises) fluctuations of angles for immotile cells, and the non-Gaussian for WT cells. The immotile cells are aligned immediately with the local flow ignoring any contribution from rotation due to shear (47). Physically, this represents the fact that immotile particles are advected by the flow, while the thrust produced by the WT cells can lead to dramatically different behavior (see Fig. S2 for direct comparison).

One apparent discrepancy between the experiment and the model can be seen in the immotile case of Fig. 4 *A*. Because the model assumes that the immotile cells are simply advected by the flow, we see approximately a δ-function in the angle between the flow and velocity, which is not present in experiment. In experiments, the local fluid flow is unknown and cannot be measured exactly. Instead, it is only observed as a local average of the moving bacteria around it. Moreover, a tracked fluorescent cell may move in a lower layer that is moving in a slightly different direction than the top one observed for the collective flow. Alternatively, this effect may be due to other factors contributing to motion in the experiment at the microscopic level that are not present in the model, such as tangling of flagella, nonpenetration during collision, and additional drag on the cell surface. Otherwise, the remaining theoretical predictions show good qualitative agreement with experiment.

In addition, Fig. 4 *D* depicts the distribution of correlations between measured angles as obtained in simulations. As observed in experiments (*smooth red curve* in Fig. 3),

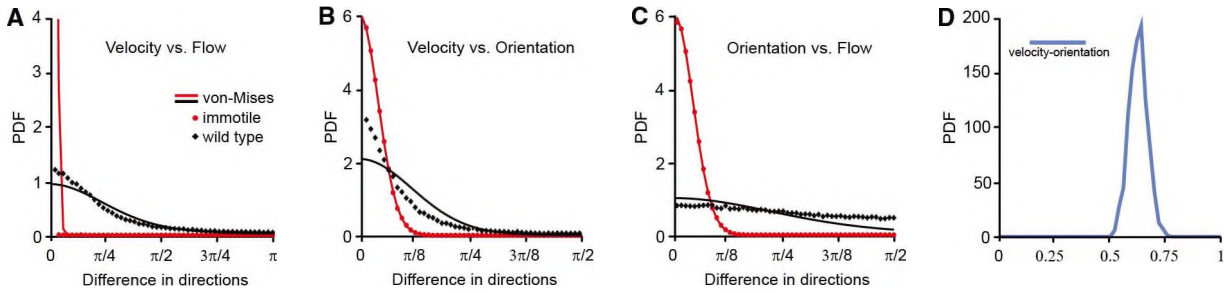

FIGURE 4 Simulation results. (*A*) Distribution of angles between the cell velocity and the flow vector field at the same position and time. Immotile cells (*pink circles*) move with the flow while WT cells (*black diamonds*) exhibit much larger deviations. (*B*) Distribution of angles between the cell velocity and its orientation. Immotile cells tend to be aligned with the actual direction of motion while WT bacteria exhibit significantly larger deviations. (*C*) Distribution of angles between cell orientation and the flow vector field at the same position and time. Immotile cells tend to be aligned with the flow while WT exhibit large deviations. (*Solid lines*) Maximal-likelihood fit to a centered von Mises distribution. (*D*) Distribution of the correlation between the velocity direction and the orientation (compared to the flow) among 1000 sample trajectories. To see this figure in color, go online.

typically, either all directions (flow, velocity, and orientation) are aligned or random. Note, however, that the distribution of correlation coefficients in experiments is significantly wider. This is expected, considering some of the highly simplifying assumptions underlying our model; for example, that all particles are identical.

To study the effect of the different contributions of the two terms in $G(x,t)$ given by Eq. 3, Fig. S3 shows simulation results with $G(x,t) = u(x,t)$ or $G(x,t) = \Delta t J(x,t)$, describing only alignment or only Jeffery (rotation due to shear) effects. Fig. S2, A–C, shows results with $G(x,t) = u(x,t)$, i.e., instantaneously alignment of the cell orientation with the local flow. Note that an elongated particle drifting within a constant flow will not rotate, but simply move with the flow, keeping its relative orientation to the flow lines. Therefore, such an alignment mechanism is biological in nature, representing a preference of cells to align with their surroundings or conspecifics. Such a tendency has been previously suggested in models of swarming (6,28). Furthermore, it may be explained by additional physical processes such as nonsymmetric repulsion between elongated particles or entanglement of flagella. The main difference between simulation results with $G(x,t) = u(x,t)$ and the experimental ones (Fig. 2) is apparent in Fig. S3 *B*, because the orientations for both the motile and immotile cells are driven toward the local flow, we see their behavior is similar. In other words, this model cannot explain the differences between WT and immotile cells observed in experiments.

Next, we take $G(x,t) = J(x,t)$ (the factor Δt does not contribute here because G is normalized; physically, this setup implies instantaneous rotation to the direction predicted by Jeffery's equation). In other words, only the hydrodynamic interaction between the elliptical shape of the particle and the local flow generated by the other cells is taken into account. In the case of linear shear flow, each cell's orientation is driven toward the direction of the shear. Simulation results, depicted in Fig. S3, *D*–F, show that this motion, combined with self-propulsion, leads to a large difference in the angles among the orientation, velocity, and flow compared to experiments. This implies that the reaction time of the cells due purely to this interaction is too slow, and that the local flow should provide a greater contribution to the orientation direction. We conclude the experimental data lies somewhere between these two approaches. Accordingly, Eq. 3 assumes a linear combination of the two mechanisms.

It is important to point out that despite its success in explaining the local directional statistics observed in experiments, our model falls short of some global dynamical characteristics of swarming bacteria. As discussed in the Introduction, it was recently shown that trajectories of swarming *B. subtilis* are superdiffusive (35), i.e., the mean-square displacement $|x(t+s) - x(s)|^2$, averaged over all times s and all sampled trajectories, is proportional to t^{α} with $\alpha > 1$ (~1.6). However, simulations with the model described above show normal diffusion. Indeed, our model is far from a complete description of the complex dynamics exhibited by swarming bacteria, and only serves to identify and interpret the key local physical processes highlighted by the experimental results. In particular, we focus on the short-range temporal and spatial neighborhood of a cell. Superdiffusion, which is observed on larger scales, is beyond the scope of our model and may require going beyond the semidilute regime including, for example, hydrodynamic interaction between streams. Additional interactions, which are not taken into account by our model include, for example, nonsymmetric steric interactions between the rod-shaped cells (49,50). These interactions have been found to play an important role in the formation of the swirl-like patterns and jets, especially in nonflagellated bacteria (51).

DISCUSSION

While swarming, each bacterium composing the colony generates thrust using its flagella to propel forward within the dense crowd. While it may naïvely be thought that the cells simply follow the flow lines that they have generated, our results have shown that the motion of bacteria is more

complicated and cells often move in directions that are perpendicular or opposed to the global flow. In addition, their orientation is not necessarily aligned with the flow direction or the direction of their motion. In contrast, immotile cells embedded in a swarm were oriented close to the flow-direction and typically moved along the flow lines. Our results clearly show that swarming bacteria use dissemination techniques that were so far undiscovered: individuals within a swarm are able to control their motion—maneuvering between streams and utilizing the swarm by generating trajectories different from those offered by the crowd.

How are individual cells able to shift off the main flow line? In a recent work (52), a confined suspension of *B. subtilis* was studied theoretically and experimentally. The cells were found to interact with both the neighboring cells and the fluids that generated the interesting result of swimming against the flow. However, individually labeled cells within the confined rotating chamber did not show motion with components perpendicular to flow lines. The exact role of flagella, while they cross field flow lines, was therefore unknown. Recent works on *Escherichia coli* swarmers (8,12) have shown that on short time- and length scales the individual motile cells are able to control some of their dynamics. In our study we have built a minimal model showing the crucial role of cell alignment due to flow and advection, and rotational diffusion due to shear flow of the neighboring cells, stemming from the propulsion thrust. Our results illustrate how the behavior of the single cells influences their own trajectories and the neighboring cells in the swarm, which dictates the overall intricate dissemination of swarming bacteria. It would be interesting to supplement these results with experiments similar to Copeland et al. (8) and Turner et al. (12), and study the relations among the large deviations in flow, velocity, and orientation reported here and the changing shape of the flagellar bundles as observed in Copeland et al. (8) and Turner et al. (12).

We have recently shown that the individual cells within a dense swarm exhibit superdiffusion, which is consistent with a Lévy walk (35). These trajectories are fundamentally different from those observed with planktonic cells or passive tracers inside a swarm (11). Together with the results presented here, these differences between the dynamical properties of active, motile cells and passive or inanimate matter open the door toward discovery and characterization of new bacterial strategies. We posit that bacteria may have evolved to take advantage of the physical properties of their surroundings (e.g., superdiffusion or anomalous fluctuations) to balance individual and group dynamics.

SUPPORTING MATERIAL

Three figures, one table, and three movies are available at http://www.biophysj.org/biophysj/supplemental/S0006-3495(16)30390-3.

AUTHOR CONTRIBUTIONS

G.A. and A.B. designed research; A.B. performed the experiments; S.D.R. and G.A. did the mathematical modeling; S.D.R., G.A., and A.B. analyzed the data; and S.D.R., G.A., and A.B. wrote the article.

ACKNOWLEDGMENTS

We thank D.B. Kearns for sending us the *B. subtilis* WT and immotile cells, A. Eldar and S. Pollak for creating the *B. subtilis* RFP mutants, R.M. Harshey for sending us the *S. marcescens* WT and immotile strains, and J.D. Partridge for creating the *S. marcescens* GFP mutants.

A.B. is thankful for partial support from European Union/FP7 REA grant No. 321777, The Israel Science Foundation's grant No. 337/12, and the Roy J. Zuckerberg Career Development Chair for Water Research.

REFERENCES

1. Harshey, R. M. 2003. Bacterial motility on a surface: many ways to a common goal. *Annu. Rev. Microbiol.* 57:249–273.
2. Partridge, J. D., and R. M. Harshey. 2013. Swarming: flexible roaming plans. *J. Bacteriol.* 195:909–918.
3. Kearns, D. B., and R. Losick. 2003. Swarming motility in undomesticated *Bacillus subtilis*. *Mol. Microbiol.* 49:581–590.
4. Kearns, D. B. 2010. A field guide to bacterial swarming motility. *Nat. Rev. Microbiol.* 8:634–644.
5. Copeland, M. F., and D. B. Weibel. 2009. Bacterial swarming: a model system for studying dynamic self-assembly. *Soft Matter.* 5:1174–1187.
6. Ariel, G., A. Shklarsh, ..., E. Ben-Jacob. 2013. From organized internal traffic to collective navigation of bacterial swarms. *New J. Phys.* 15:125019.
7. Butler, M. T., Q. Wang, and R. M. Harshey. 2010. Cell density and mobility protect swarming bacteria against antibiotics. *Proc. Natl. Acad. Sci. USA.* 107:3776–3781.
8. Copeland, M. F., S. T. Flickinger, ..., D. B. Weibel. 2010. Studying the dynamics of flagella in multicellular communities of *Escherichia coli* by using biarsenical dyes. *Appl. Environ. Microbiol.* 76:1241–1250.
9. Tuson, H. H., M. F. Copeland, ..., D. B. Weibel. 2013. Flagellum density regulates *Proteus mirabilis* swarmer cell motility in viscous environments. *J. Bacteriol.* 195:368–377.
10. Patrick, J. E., and D. B. Kearns. 2008. MinJ (YvjD) is a topological determinant of cell division in *Bacillus subtilis*. *Mol. Microbiol.* 70:1166–1179.
11. Be'er, A., and R. M. Harshey. 2011. Collective motion of surfactant-producing bacteria imparts superdiffusivity to their upper surface. *Biophys. J.* 101:1017–1024.
12. Turner, L., R. Zhang, ..., H. C. Berg. 2010. Visualization of flagella during bacterial Swarming. *J. Bacteriol.* 192:3259–3267.
13. Roth, D., A. Finkelshtein, ..., E. Ben-Jacob. 2013. Identification and characterization of a highly motile and antibiotic refractory subpopulation involved in the expansion of swarming colonies of *Paenibacillus vortex*. *Environ. Microbiol.* 15:2532–2544.
14. Benisty, S., E. Ben-Jacob, ..., A. Be'er. 2015. Antibiotic induced anomalous statistics of collective bacterial swarming. *Phys. Rev. Lett.* 114:018105.
15. Zhang, H. P., A. Be'er, ..., H. L. Swinney. 2009. Swarming dynamics in bacterial colonies. *Europhys. Lett.* 87:48011.
16. Zhang, H. P., A. Be'er, ..., H. L. Swinney. 2010. Collective motion and density fluctuations in bacterial colonies. *Proc. Natl. Acad. Sci. USA.* 107:13626–13630.
17. Chen, X., X. Dong, ..., H. P. Zhang. 2012. Scale-invariant correlations in dynamic bacterial clusters. *Phys. Rev. Lett.* 108:148101.

18. Be'er, A., R. S. Smith, ..., H. L. Swinney. 2009. *Paenibacillus dendritiformis* bacterial colony growth depends on surfactant but not on bacterial motion. *J. Bacteriol.* 191:5758–5764.

19. Be'er, A., S. K. Strain, ..., E.-L. Florin. 2013. Periodic reversals in *Paenibacillus dendritiformis* swarming. *J. Bacteriol.* 195:2709–2717.

20. Darnton, N. C., L. Turner, ..., H. C. Berg. 2010. Dynamics of bacterial swarming. *Biophys. J.* 98:2082–2090.

21. Ingham, C. J., and E. Ben Jacob. 2008. Swarming and complex pattern formation in *Paenibacillus vortex* studied by imaging and tracking cells. *BMC Microbiol.* 8:36.

22. Sokolov, A., and I. S. Aranson. 2012. Physical properties of collective motion in suspensions of bacteria. *Phys. Rev. Lett.* 109:248109.

23. Dunkel, J., S. Heidenreich, ..., R. E. Goldstein. 2013. Fluid dynamics of bacterial turbulence. *Phys. Rev. Lett.* 110:228102.

24. Rabani, A., G. Ariel, and A. Be'er. 2013. Collective motion of spherical bacteria. *PLoS One.* 8:e83760.

25. Sokolov, A., I. S. Aranson, ..., R. E. Goldstein. 2007. Concentration dependence of the collective dynamics of swimming bacteria. *Phys. Rev. Lett.* 98:158102.

26. Cisneros, L. H., R. Cortez, ..., J. O. Kessler. 2007. Fluid dynamics of self-propelled microorganisms, from individuals to concentrated populations. *Exp. Fluids.* 43:737–753.

27. Sokolov, A., and I. S. Aranson. 2009. Reduction of viscosity in suspension of swimming bacteria. *Phys. Rev. Lett.* 103:148101.

28. Wensink, H. H., J. Dunkel, ..., J. M. Yeomans. 2012. Meso-scale turbulence in living fluids. *Proc. Natl. Acad. Sci. USA.* 109:14308–14313.

29. Saintillan, D., and M. J. Shelley. 2007. Orientational order and instabilities in suspensions of self-locomoting rods. *Phys. Rev. Lett.* 99:058102.

30. Aditi Simha, R., and S. Ramaswamy. 2002. Hydrodynamic fluctuations and instabilities in ordered suspensions of self-propelled particles. *Phys. Rev. Lett.* 89:058101.

31. Wolgemuth, C. W. 2008. Collective swimming and the dynamics of bacterial turbulence. *Biophys. J.* 95:1564–1574.

32. Sambelashvili, N., A. W. C. Lau, and D. Cai. 2007. Dynamics of bacterial flow: emergence of spatiotempral coherent structures. *Phys. Lett. A.* 360:507–511.

33. Sankararaman, S., and S. Ramaswamy. 2009. Instabilities and waves in thin films of living fluids. *Phys. Rev. Lett.* 102:118107.

34. Aranson, I. S., A. Sokolov, ..., R. E. Goldstein. 2007. Model for dynamical coherence in thin films of self-propelled microorganisms. *Phys. Rev. E Stat. Nonlin. Soft Matter Phys.* 75:040901.

35. Ariel, G., A. Rabani, ..., A. Be'er. 2015. Swarming bacteria migrate by Levy walk. *Nat. Comm.* 6:8396.

36. Gyrya, V., I. S. Aranson, ..., D. Karpeev. 2010. A model of hydrodynamic interaction between swimming bacteria. *Bull. Math. Biol.* 72:148–183.

37. Lin, S. N., W. C. Lo, and C. J. Lo. 2014. Dynamics of self-organized rotating spiral-coils in bacterial swarms. *Soft Matter.* 10:760–766.

38. Baskaran, A., and M. C. Marchetti. 2009. Statistical mechanics and hydrodynamics of bacterial suspensions. *Proc. Natl. Acad. Sci. USA.* 106:15567–15572.

39. Berg, H. C. 2004. E. coli in Motion. Springer Science & Business Media USA, New York.

40. Ryan, S. D., B. M. Haines, ..., I. S. Aranson. 2011. Viscosity of bacterial suspensions: hydrodynamic interactions and self-induced noise. *Phys. Rev. E Stat. Nonlin. Soft Matter Phys.* 83:050904, (R).

41. Ryan, S. D., L. Berlyand, ..., D. Karpeev. 2013. A kinetic model for semidilute bacterial suspensions. *SIAM Multiscale Model. Simul.* 11:1176–1196.

42. Ryan, S. D., A. Sokolov, ..., I. S. Aranson. 2013. Correlation properties of collective motion in bacterial suspensions. *New J. Phys.* 15:105021.

43. Horn, B. K. P., and B. G. Schunck. 1981. Determining optical flow. *Artif. Intell.* 17:185–203.

44. Saintillan, D., and M. Shelley. 2013. Active suspensions and their nonlinear models. *C. R. Phys.* 14:497–517.

45. Hernández-Ortiz, J. P., P. T. Underhill, and M. D. Graham. 2009. Dynamics of confined suspensions of swimming particles. *J. Phys. Condens. Matter.* 21:204107.

46. Drescher, K., J. Dunkel, ..., R. E. Goldstein. 2011. Fluid dynamics and noise in bacterial cell-cell and cell-surface scattering. *Proc. Natl. Acad. Sci. USA.* 108:10940–10945.

47. Jeffery, G. B. 1922. The motion of ellipsoidal particles immersed in a viscous fluid. *Proc. Roy. Soc. London A Math. Phys. Eng. Sci.* 102:161–179.

48. Cui, B., H. Diamant, ..., S. A. Rice. 2004. Anomalous hydrodynamic interaction in a quasi-two-dimensional suspension. *Phys. Rev. Lett.* 92:258301.

49. Peruani, F., A. Deutsch, and M. Bär. 2006. Nonequilibrium clustering of self-propelled rods. *Phys. Rev. E Stat. Nonlin. Soft Matter Phys.* 74:030904.

50. Weitz, S., A. Deutsch, and F. Peruani. 2015. Self-propelled rods exhibit a phase-separated state characterized by the presence of active stresses and the ejection of polar clusters. *Phys. Rev. E Stat. Nonlin. Soft Matter Phys.* 92:012322.

51. Peruani, F., J. Starruss, ..., M. Bär. 2012. Collective motion and nonequilibrium cluster formation in colonies of gliding bacteria. *Phys. Rev. Lett.* 108:098102.

52. Lushi, E., H. Wioland, and R. E. Goldstein. 2014. Fluid flows created by swimming bacteria drive self-organization in confined suspensions. *Proc. Natl. Acad. Sci. USA.* 111:9733–9738.